Climate response to increasing Antarctic iceberg and ice shelf melt

Shona Mackie*

Department of Physics, University of Otago, Dunedin, New Zealand

Inga J. Smith

Department of Physics, University of Otago, Dunedin, New Zealand

Jeff K. Ridley

Met Office, Exeter, U.K.

David P. Stevens

School of Mathematics, University of East Anglia, Norwich, U.K.

Patricia J. Langhorne

Department of Physics, University of Otago, Dunedin, New Zealand

**Corresponding author address:* Department of Physics, University of Otago, Dunedin 9016, New Zealand

E-mail: shona.mackie@otago.ac.nz

ABSTRACT

Mass loss from the Antarctic continent is increasing, however climate models either assume a constant mass loss rate, or return snowfall over land to the ocean to maintain equilibrium. Numerous studies have investigated sea ice and ocean sensitivity to this assumption and reached different conclusions, possibly due to different representations of melt fluxes. The coupled atmosphere-land-ocean-sea ice model, HadGEM3-GC3.1, includes a realistic spatial distribution of coastal melt fluxes, a new ice shelf cavity parametrization and explicit representation of icebergs. This makes it appropriate to revisit how increasing melt fluxes influence ocean and sea ice, and to assess whether responses to melt from ice shelves and icebergs are distinguishable. We present results from simulated scenarios of increasing meltwater fluxes and show that these drive sea ice increases and, for increasing ice shelf melt, a decline in Antarctic Bottom Water formation. In our experiments, the mixed layer around the Antarctic coast deepens in response to rising ice shelf meltwater, and shallows in response to stratification driven by iceberg melt. We find similar surface temperature and salinity responses to increasing meltwater fluxes from ice shelves and icebergs, but mid-layer waters warm to greater depths and further north when ice shelf melt is present. We show that as meltwater fluxes increase, snowfall becomes more likely at lower latitudes, and Antarctic Circumpolar Current transport declines. These insights are helpful for interpretation of climate simulations that assume constant mass loss rates, and demonstrate the importance of representing increasing melt rates for both ice shelves and icebergs.

1. Introduction

Earth system models (ESMs) link physical processes on land, sea ice, ocean and atmosphere and the feedbacks between them. In addition to calculating the likely future climate, ESMs are excellent tools for investigating the sensitivity of the climate system to specific processes, providing insights useful for understanding responses to future change. An example of this is the rate at which ice mass is lost from Antarctica, which is the focus of this study. Mass loss from Antarctica has increased in recent years (Rignot et al. 2008; Sutterley et al. 2014; Williams et al. 2014; Martin-Espanol et al. 2016; Shepherd et al. 2018), and is likely to continue to increase (Timmermann and Hellmer 2013). Coupling a dynamic ice sheet model with an ESM to realistically capture the changing mass loss rate is technically complex, and most ESMs therefore share the assumption that the rate of mass loss is temporally constant. It is important to understand the effects of this assumption on future climate projections, so as to interpret them appropriately.

Almost all mass loss from the Antarctic continent, with the exception of sublimation, enters the ocean as meltwater. Surface runoff, ice shelf basal melt and icebergs affect ocean stability and sea ice processes. Near-surface atmosphere, ocean and sea ice properties and processes are spatially variable, making the ocean and sea ice response to melt fluxes spatially variable. For example, in recent years, Antarctic sea ice extent has increased in some areas and decreased in others (Cavalieri and Parkinson 2008; Turner et al. 2009; Comiso et al. 2011; Pezza et al. 2012; Williams et al. 2014; Parkinson 2019). An appropriate spatial distribution of melt fluxes is therefore likely to be necessary for an accurate representation of their effects on sea ice and the ocean. This should capture the relative melt rates around the Antarctic coast, and include the effects of iceberg melt, which enters the ocean with a seasonality and spatial distribution dependent on ocean surface properties (and is therefore coupled to atmosphere and ocean processes) (Merino et al. 2016).

There are different responses to melt entering the ocean at depth along ice shelf fronts (most ice shelf melt occurs at the grounding line), and at the surface, for example as iceberg melt (Pauling et al. 2016). Melt entering the ocean at depth is buoyant and rises to the surface, potentially becoming supercooled due to the pressure changes as it does so. The ocean is generally modelled with the surface forming a boundary, and then layers that become thicker as depth increases. The cavity beneath an ice shelf is usually not represented in ESMs because of the technical difficulty of making the cavity shape sensitive to changes in water temperature while avoiding instabilities around the grounding line (Losch 2008). Nonetheless, the modification of surface waters, driven by ice shelf basal melt, can contribute to sea ice formation, and an appropriate representation of melt along ice shelf fronts is needed to accurately represent sea ice processes.

The net of precipitation minus evaporation (P - E) provides the largest freshwater flux to the Southern Ocean (Pauling et al. 2017), and increases can result in increased sea ice concentration (Purich et al. 2018). In the absence of mechanical mixing driven by wind and waves, freshwater from any source can form a buoyant low salinity layer atop the more saline water, increasing the heat content of mid-layer ocean waters, which are then prevented from ventilating and exchanging heat with the atmosphere (Hellmer 2004; Richardson et al. 2005; Morrison et al. 2015). Sea ice growth is enhanced by this freshwater-induced stratification, as well as by the higher freezing temperature of the freshwater, and increases in Antarctic melt fluxes are therefore likely to drive increases in sea ice (Turner et al. 2013; Bintanja et al. 2013; Swart and Fyfe 2013; Bintanja et al. 2015; Zunz and Goosse 2015; Pauling et al. 2016, 2017; Bronselaer et al. 2018). The lower atmosphere may be impacted by surface temperature changes driven by the stratification and by changes to the sea ice through the sea ice albedo feedback.

Changes in sea ice may impact on the Southern Annular Mode (SAM), one characteristic of which is the changing latitudinal position of the westerly circumpolar winds surrounding Antarctica, the so-called westerly jet. The position of the jet affects mid-latitude weather, and the winds themselves influence the carbon uptake of the ocean (Hoskins and Hodges 2005; Le Quéré et al. 2007). The meridional temperature gradient is projected to steepen under future climate scenarios, driving a strengthening and polewards shift of the jet (Bracegirdle et al. 2013). However, the jet strength and position are also affected by changes in sea ice cover (Bracegirdle et al. 2018), and so may be impacted by changes to freshwater fluxes entering the Southern Ocean.

Many ocean processes are sensitive to freshwater and sea ice, and can only be accurately represented if melt fluxes are appropriately represented. For example, freshwater-induced stratification and warming of the subsurface ocean can cause density changes that impact on ocean currents and water formation. Brine rejection during sea ice production can generate High Salinity Shelf Water (HSSW). In key regions, HSSW can sink and spill over the edge of the continental shelf into the deep ocean as Antarctic Bottom Water (AABW). AABW spreads northwards and mixes in the abyssal gyres to upwell at lower latitudes and travel polewards as Circumpolar Deep Water (Sloyan 2006). This overturning is a driver of the thermohaline circulation, the primary mechanism by which heat moves around the world's oceans (Weaver et al. 2003; Marsland et al. 2007). AABW production and global ocean circulation may therefore be sensitive to meltwater-induced changes in sea ice (Lago and England 2019; Weaver et al. 2003; Marsland et al. 2007; Ronald et al. 2007). An analogous process in the northern hemisphere drives the Atlantic Meridional Overturning Circulation (AMOC). The AMOC is important to northern hemisphere climate (Buckley and Marshall 2016; Sévellec and Fedorov 2016), and is projected to decline as the climate warms (Rahmstorf et al. 2015). Links between the two overturning cells have been found; for example Weaver et al. (2003) found a freshwater perturbation in the southern hemisphere resulted in reduced AABW production, which "reactivated" the AMOC from an "off" state, providing a mechanism by which changes to Antarctic sea ice could impact on northern hemisphere climate, and other studies have also found northern hemisphere changes to result from an Antarctic meltwater perturbation (Richardson et al. 2005; van den Berk et al. 2019).

Recent ESM developments allow icebergs to be explicitly represented and their transport and melt coupled to ocean surface properties (Marsh et al. 2015). This make it possible to more appropriately apportion the mass loss from grounded ice between icebergs and ice shelf melt than previously in a coupled model. Combined with updated glaciological estimates of the spatial distribution of Antarctic mass loss (Depoorter et al. 2013; Rignot et al. 2013), and an improved vertical representation of ice shelf melt (Mathiot et al. 2017), it is appropriate to reassess sea ice and ocean responses to increased mass loss scenarios. Merino et al. (2018) investigated this using a coupled ocean-sea ice model with Antarctic mass loss realistically distributed between ice shelves around the Antarctic coast. At each ice shelf, the mass flux was proportioned between melt at the ice shelf front and a calving term for a dynamic iceberg model, using glaciological estimates of calving rates and ice shelf melt. Reanalysis data provided atmospheric forcing. That study found strong regional variations in the sea ice response, highlighting the significance of a realistically distributed melt flux. The findings in Merino et al. (2018) are an important advance in understanding, however the study made several simplifications which we hope to address here. Sea ice and ocean interactions with the atmosphere have been shown to be important to sea ice processes (Stammerjohn et al. 2008), and the forced atmosphere in Merino et al. (2018) means that these feedbacks were neglected. The use of atmospheric forcing also necessitated salinity restoration and, although this was mostly implemented beyond the northern sea ice edge, freshwater forcing around Antarctica has been shown to affect ocean properties further north (Richardson et al. 2005). Lastly, the freshwater perturbation in Merino et al. (2018) was fixed, whereas the changing mass balance of Antarctic ice shelves show that it is accelerating in at least some places (Sutterley et al. 2014; Paolo et al. 2015). Implementing a changing melt flux in a coupled model may reveal additional processes to those seen under a constant melt flux. Recently, Bronselaer et al. (2018) used climate projections from the CMIP5 experiment as external forcings for an ice sheet model, and so calculated increases in Antarctic mass loss realistic for an assumed future emissions scenario. The calculated mass loss rates were distributed uniformly around the coast as a surface melt flux in an ESM, and ocean and sea ice responses were assessed. While those findings provide useful insights into likely future changes driven by increased Antarctic melt, the results depend on the assumed future emissions scenario and do not account for meltwater entering the ocean at depth or with a non-uniform spatial distribution, which is likely to impact local sea ice. A study by Schloesser et al. (2019) highlights the importance of icebergs to the distribution of meltwater entering the Southern Ocean. An ice sheet model was used to partition Antarctic mass loss between icebergs and meltwater entering the ocean at the coastal ice shelves. Future emissions scenarios provided external forcings to assess the likely effect of icebergs and ice shelf melt on future climate. In that work, the two meltwater pathways resulted in different effects on surface ocean and atmosphere temperatures, and iceberg meltwater effects were found to depend on the size of the icebergs and on the ocean properties that determined their trajectories. Using future emissions scenarios makes that study a useful indicator of future climate under different scenarios, but it is not straightforward to isolate effects attributable to the increasing meltwater fluxes from those attributable to changes in other external forcings (for example, interactions between effects from increasing CO_2 and from increasing meltwater fluxes are non-linear (Mackie et al. submitted)). Furthermore, Schloesser et al. (2019) did not include a parametrization for the ice shelf cavity and considered both ice shelf and iceberg meltwater as a surface flux. In reality, icebergs are rarely as deep as ice shelf grounding lines, where most ice shelf melt occurs, and meltwater entering the ocean at depth may have different effects to a surface meltwater flux (Pauling et al. 2016).

Here, we investigate sea ice and ocean responses to an increasing rate of Antarctic mass loss. We implement the dynamic iceberg scheme from Marsh et al. (2015) in a fully coupled atmosphere-ocean-sea ice climate model. To our knowledge, this is the first study into the sensitivity of a fully coupled climate model to an increasing rate of mass loss from Antarctica, where icebergs are explicitly represented and the melt flux is distributed using a realistic spatial distribution and an improved parametrization of the ice shelf cavity. We isolate the sensitivity to increasing meltwater by assuming an unchanging pre-industrial emissions scenario and investigate the effect of the increasing Antarctic mass loss rate (a further experiment assesses the sensitivities in the context of increasing CO_2 levels (Mackie et al. submitted)). We also examine whether the role of ice shelf melt on ocean and sea ice characteristics is distinguishable from that of iceberg melt.

2. Method

Model Description

We use the coupled land-ocean-atmosphere-sea ice model, HadGEM3-GC3.1 (Williams et al. 2017; Kuhlbrodt et al. 2018). We refer to Storkey et al. (2018) for a description of the ocean component, GO6 (based on NEMO (Madec and team 2016)) and to Ridley et al. (2018) for a description of the sea ice component, GSI8.1 (based on CICE 5 (Hunke et al. 2015)). Melt-freeze processes in GSI8.1 depend on ocean salinity, so freshening the surface waters is anticipated to lead to increased sea ice concentration. The simulations use the ORCA1 grid (nominally 1° resolution) for the ocean and sea ice components, and an atmospheric resolution of 1.875° by 1.25°, with 75 vertical layers in the ocean, and 85 levels for the atmosphere. In the standard configuration, the rate of Antarctic mass loss remains constant at 1770.75 Gt / year. This figure was calculated as the rate of mass loss, assumed constant, that would keep the Antarctic ice sheets in mass balance in the model over 100 years with pre-industrial forcings, and consequently results in no ocean salinity drift (in simulations of future climate change, increasing accumulation over Antarctica will intentionally result in sea level fall). A small amount of accumulation is lost through sublimation and surface melt (determined by atmospheric conditions over the continent), and the remainder is distributed as a mass flux that enters the ocean through ice shelves around the Antarctic coast (the latter processes dominate the mass loss mechanism by several orders of magnitude (Liston and Winther 2005)), proportioned between these according to the distribution in Rignot et al. (2013). At each ice shelf, an iceberg calving flux accounts for 45% of the mass loss and 55% is depicted as ice shelf basal melt. The ice shelf cavity is not explicitly represented, instead basal melt enters the ocean at the ice shelf front, distributed evenly between model levels spanning the vertical range of the ice shelf draft, following the parametrization in Mathiot et al. (2017). The Lagrangian iceberg scheme (Marsh et al. 2015) creates icebergs at the ice shelf front using the size distribution from Bigg et al. (1997), with horizontal dimensions from 100 m x 67 m up to 1.5 km x 1 km. Simulated icebergs must be small relative to a model grid cell (cells become smaller at high latitudes) because they exist only as a meltwater source and are effectively 'invisible', i.e., solar radiation reaching the ocean is not impacted by their presence. Once calved, iceberg motion is determined by drag on the iceberg from the atmosphere, ocean and sea ice (a wave radiation forcing is also applied, following Martin and Adcroft (2010)). The drift of modelled icebergs may be slowed sufficiently to represent their becoming grounded. There is no momentum exchange between icebergs and sea ice, and sea ice is unaffected by the icebergs. The dominant mechanism for iceberg decay is wave erosion, but this only occurs when the icebergs are surrounded by ocean, and decreases linearly with increasing sea ice concentration to be zero when an iceberg is in a grid cell with 100% sea ice cover (Martin and Adcroft 2010). Model iceberg decay is otherwise accounted for by basal melt, determined by the ocean surface temperature plus 4° C (to approximate the temperature at 500 m depth). The latent heat associated with iceberg melt cools the surface ocean. Modifications to improve this scheme and allow icebergs to interact with the subsurface ocean have been proposed (Merino et al. 2016), but are not included in HadGEM3-GC3.1, and icebergs in our study do not interact with the subsurface ocean. Processes for mass loss in the Arctic are similar, with mass loss from the Greenland Ice Sheet fixed at a constant rate. However, in HadGEM3-GC3.1 Greenland is assumed to have no ice shelves, and so the residual from the surface mass balance enters the ocean solely as icebergs.

Experiments

Three experiments were undertaken to assess the effect of an increasing rate of Antarctic mass loss, relative to the HadGEM3-GC3.1 pre-industrial control simulation submitted to CMIP6 (PIControl). In all the experiments, the total rate of mass loss increases by 2.33% each year for 100 years, so that the final rate is ten times the initial rate (Figure 1). The scenario was designed to look at the sensitivity of the modelled ocean and sea ice to the increasing rate of mass loss, rather than to be realistic in terms of absolute numbers. For context, however, the freshwater contribution from Antarctica to the Southern Ocean could rise above 1 Sv (31104 Gt / year using HadGEM3-GC3.1's 360 day model year) by the year 2100 under RCP 8.5 (DeConto and Pollard 2016; Schloesser et al. 2019; van den Berk et al. 2019), which is almost twice the maximum reached in our experiments (17707.5 Gt / year). Mass loss from the Greenland Ice Sheet remains as per the standard model in all experiments, and all forcings other than Antarctic mass loss are equal to those in PIControl. The first experiment, FW, investigates the sensitivity of the modelled ocean and sea ice to the increasing mass loss, proportioning the loss at the coast between ice shelf melt and an iceberg calving flux as for PIControl. The second and third experiments, FWShelf and FWBerg, consider whether effects attributable to increasing iceberg and to ice shelf melt can be differentiated. The iceberg calving rate for Antarctic ice shelves is highly variable, but is assumed constant in the standard configuration. If we can distinguish between the climate response to increased melt at ice shelf fronts and increased melt from icebergs, then it may be appropriate to find a more detailed parametrization for iceberg melt, and there may be implications for projections from climate models without explicit iceberg representation. In the southern hemisphere, no icebergs are calved in FWShelf and all melt enters the ocean as ice shelf basal melt, while in FWBerg there is no ice shelf melt and all mass loss enters the ocean at the surface as an iceberg melt flux. FWShelf and FWBerg isolate responses separately attributable to iceberg or ice shelf melt, but in reality (and in FW), the effects of iceberg and ice shelf melt are not independent (ice shelf melt may cool surface waters and so inhibit iceberg melt). Configurations for the experiments are summarised in Table 1, and the data are available at Mackie et al. (2020). The drift in the PIControl is about 0.01 K per Century. Where anomalies are used to show differences between the experiments and PIControl, the values compared represent averages over multiple years and no fitting is performed. Anomalies are computed by subtracting the PIControl value from the value for the same diagnostic in the experiment for the equivalent model time period. Otherwise, the experiments and PIControl are presented as timeseries of absolute values, rather than as anomalies.

The mean spatial distribution of the melt flux in PIControl is shown alongside the anomaly for the final 20 years of FW in Figure 2. The spatial distribution of ice shelf melt and iceberg calving is unchanged throughout the experiments, although icebergs may follow different trajectories and so alter the iceberg melt distribution.

3. Results

Sea Ice Area and Volume

Sea ice area (SIA) increased in all the experiments, however there was no shift in the timing of the seasonal cycle (with the caveat that these data represent monthly averages) as a result of the melt anomaly (Figure 3). This is perhaps surprising, since iceberg melt introduces a seasonality that is enhanced in FWBerg, and removed altogether in FWShelf. Antarctic sea ice trends are spatially variable (Cavalieri and Parkinson 2008), and so we consider the sea ice response separately for the different ocean sectors in Figure 4 (sectors follow Yuan et al. (2017)). The total melt flux and the sea ice area (SIA) for the experiments and for PIControl is plotted for these sectors in Figures 6 and 5, and discussed in the following paragraphs.

In all the experiments, SIA follows PIControl initially, and then increases in all sectors (Figure 5). The only differences between the effects driven by the different melt sources are the timing and magnitude of the increase. In FWShelf, the increase in SIA begins earlier than in FW and FWBerg where the time taken for icebergs to melt introduces a delay (icebergs also have the effect of displacing the melt flux so that some of it enters the ocean further north, where it is less likely to impact sea ice growth). FWShelf therefore results in the strongest SIA impact, and FWBerg the weakest (and most variable), with FW driving a response in between the two.

In all three experiments, the SIA response in Figure 5 is stronger in the Ross Sea sector than in the Indian Ocean and Western Pacific, despite similar increases in the volume of melt input in these regions (Figure 6). The meltwater received by the Ross Sea sector is likely to be supplemented by both ice shelf melt and icebergs transported from the Amundsen-Bellinghausen Sea by the coastal current and the Ross Gyre, resulting in a stronger SIA response in the Ross Sea than can be attributed solely to increases in local ice shelf melt and melt from locally calved icebergs. The transport of icebergs means that FWBerg results in very little, if any, additional melt entering the Amundsen-Bellinghausen Sea relative to PIControl. In FWShelf, the additional melt entering the Amundsen-Bellinghausen Sea sector is higher than in other sectors, but the SIA response is relatively weak as some of the meltwater is transported out of the sector similarly to the icebergs. The additional melt volume received by the Weddell Sea and Indian Ocean sectors in FWBerg is much greater than in FWShelf, suggesting that icebergs enter these areas from elsewhere. The magnitude of the SIA response, however, is similar for all three experiments in these sectors, since a high proportion of the icebergs in these regions melt further north (Figure 2), where they are less likely to impact sea ice growth. The SIA response is weakest in the Western Pacific for all experiments, and all three experiments correspond to similar increases in melt here (relative to PIControl).

Local differences in the sea ice response to FWShelf and FWBerg indicate areas where sea ice growth is primarily driven by ice shelf melt. These areas are less accessible to icebergs, and/or have surface water that is cold enough (without ice shelf melt-induced cooling) to suppress iceberg melt. By the end of FWShelf, sea ice thickening is particularly strong along the Amundsen-Bellinghausen Sea coast and the eastern coast of the Antarctic Peninsula, where ice shelf basal melt is strongest (Figure 7). FWShelf also has a sea ice thickness anomaly at the continental shelf break and along the eastern coast in the Ross Sea that is largely absent in FWBerg (see Figure 4 for bathymetry). In the earlier part of FWBerg (Figure S1 in Supplemental Material), there is a slight reduction in ice concentration in the northern Ross Sea, indicating that growth here is initially driven by the ice shelf melt that is absent in FWBerg. Along the western coast of the Antarctic Peninsula, the earlier part of FWShelf results in a small decrease in ice concentration, suggesting that icebergs are important to sea ice growth here. The different spatial distribution of the thickness response does not directly follow the distribution of the meltwater input. For example, thickening northwards from the coast, where the meltwater input is higher in FWBerg, is much stronger in FWShelf than FWBerg, due to advection of the ice shelf meltwater.

Sea Ice Formation Processes

To assess which sea ice processes were enhanced or inhibited by the additional meltwater, sea ice volume anomalies attributed to specific growth and decay processes were examined. The full volume budget includes growth through frazil formation, congelation, and snow-to-ice conversion, and decay through top, lateral and basal melt, and surface sublimation. Snow-to-ice conversion, lateral melt, sublimation and top surface melt remained largely unchanged in the experiments and we therefore only discuss changes to the other budget terms. Congelation growth is the downwards growth (thickening) of existing sea ice into the ocean, due to the atmosphere-ocean temperature difference. As the ice thickens, the temperature gradient through the ice weakens and congelation growth declines (Figure S2 in Supplemental Material shows the relationship between thickness and congelation growth rate). Frazil growth is the freezing of ice crystals that have accumulated at the ocean surface, or beneath existing sea ice. In the model, these ice crystals are formed when surface waters are supercooled (in the real world, supercooling can also lead frazil to form at depth (Smith et al. 2001, 2012; Langhorne et al. 2015)). Figure 8 shows the change in the proportion of the sea ice volume budget that is accounted for by these different processes.

In all three experiments, congelation growth is initially unaffected by the additional melt, but becomes inhibited as the sea ice thickens, altering the temperature gradient through the ice. FWShelf shows the greatest reduction in congelation growth, corresponding to the strongest thickening. Sea ice basal melt decreases as it depends on the freeze/melt temperature of the surface waters, which increases in all three experiments as the water freshens. Reduced sea ice basal melt therefore increases the sea ice volume similarly in all experiments. Frazil production increases in response to the rising of the increased volumes of supercooled melt entering the ocean at depth along the ice shelf fronts in FWShelf and FW, and additionally in response to a local overturning driven by this rising meltwater (discussed in Section 3). The frazil response is therefore stronger, and begins earlier, in the experiments that include ice shelf melt in Figure 8. Some increase in frazil production occurs in FWBerg (Figure 8c) in response to increased sea ice growth at the fringes of the ice pack where iceberg melt raises the freezing temperature of the ocean surface. In all three experiments, reduced sea ice basal melt contributes strongly to sea ice growth, but frazil production is the dominant driver for growth in experiments that include ice shelf melt.

Water Mass Formation

The additional meltwater in the experiments may change where sea ice forms, with implications for water mass formation associated with sea ice production. The salt flux into the ocean from sea ice freeze/melt can be used to discriminate areas of sea ice production in the model. Although sea ice is relatively fresh, the finite salt budget of the ocean means that freezing ocean is associated with a negative salt flux (since salt is removed, albeit in low concentration relative to the volume of water removed). Conversely, melting sea ice corresponds to a positive flux since the salt is returned to the ocean. The salt flux is therefore a proxy for sea ice growth, and a negative (positive) anomaly indicates increased (reduced) sea ice growth. The converse applies for melt (Figure 9). In PIControl, most ice production occurs in shore leads on the coast (dark blue areas), and southerly winds force the ice northwards, where it thickens further (lighter blue areas). At the northern extent of the sea ice, the ice melts, creating a ‘melt-edge’ (shaded red because salt from the ice is returned to the ocean). In the experiments, the melt-edge has moved north. There are some differences between the sea ice production response over the continental shelf in FWShelf and FWBerg (see Figure 4 for bathymetry). For example, in the Ross Sea and close to the coast in the Weddell Sea, production increases in FWShelf (Figure 9b) and decreases slightly in FWBerg (Figure 9c).

Sea ice production is often associated with a deepening mixed layer, as brine rejection creates sinking dense saline water that drives convection. This can be countered by high basal melt rates at some ice shelf fronts that inhibit the salinity-driven deepening of the mixed layer and associated deep convection (Silvano et al. 2018). However, in FWShelf there is a deepening of the mixed layer close to the coast, despite high ice shelf basal melt rates, even in areas where sea ice production has not increased (Figure 10). This deepening around the coast, which does not occur in FWBerg, reflects a local overturning driven by the high volume of ice shelf melt entering the ocean at depth and rising to the surface in FWShelf, as also found in Pauling et al. (2016) and explained in Merino et al. (2018). As ice shelf melt increases, the overturning strengthens and more heat is pumped from deeper ocean layers and advected toward the surface in front of the ice shelves, reducing the sea ice volume near the ice shelf margins. This encourages shore leads to form, where latent heat release generates more frazil (Figure 8), which then increases sea ice production (Jourdain et al. 2017). In contrast, FWBerg results in a shallowing of the mixed layer around the coast, including in areas of increased sea ice production such as along the eastern Indian Ocean-western Weddell Sea coastline, and along the western coast of the Antarctic Peninsula. The large increase in surface meltwater from icebergs here stratifies the ocean, in agreement with (Pauling et al. 2016), and saline rejection is too diffuse to generate large scale circulation changes.

The dense sinking water associated with sea ice production can spill over the shelf edge into the deep ocean as AABW. The Weddell and Ross Seas and the Adelie coast in the Western Pacific are the dominant sources of AABW production in the real ocean (M. van Aken 2007; Nicholls et al. 2009). The changes to sea ice production and mixed layer depth in these regions may therefore impact on AABW formation. To assess this, we define the AABW transport as the net zonal mean northward transport of the bottom waters at 30° S (following Heuzé et al. (2015)). We assume that any reduction (increase) in AABW formation will be reflected in a reduction (increase) in the northwards export of AABW (Figure 11a). To assess any impact on the AMOC we follow Heuzé et al. (2015) and define the AMOC strength as the maximum of the depth-integrated meridional transport through the Atlantic basin at 30° S in the southward direction (Figure 11b).

Both FWShelf and FW (FW not shown) result in an overall increase in sea ice production over the continental shelf (Figure 9b), however this is associated with a decrease in AABW formation relative to PIControl. This reduction follows from the freshening of the whole water column over the shelf seas in response to the large additional melt flux that enters at the ice shelf fronts. This freshening can be seen in the evolution of the salinity response for the ocean south of 60° S for FWShelf and FW, but not for FWBerg, where meltwater enters at the ocean surface and is more widely distributed (Figure 12). This agrees with findings presented in Silvano et al. (2018), but contrasts with the findings from Lago and England (2019), who used a coupled ocean-sea ice model driven by climatological atmospheric forcing to assess the impact of Antarctic melt fluxes on AABW production. The melt fluxes in Lago and England (2019) all entered the ocean at the surface (not at depth as in FW and FWShelf here and in Silvano et al. (2018)) and induced a stratification that resulted in a decline in AABW formation over the continental shelf. In this study, the stratification induced by surface melt fluxes in FWBerg (Figure 10) is not enough to reduce AABW formation, and we see a decline only when melt enters the ocean at depth and freshens the water column.

The impact of this reduction in AABW formation on the AMOC appears small in Figure 11b, and so we used a student t-test to compare the experiments with PIControl for the final 20 years of the simulations. Over the final 20 years of the simulations, the AMOC has an average strength of 14.22 Sv in PIControl, and this is 0.43 and 0.35 Sv stronger in FW and FWShelf, respectively at the 95 % confidence level. There is no statistically significant change to the AMOC strength in FWBerg (the p-value is greater than 0.7).

Surface Ocean

Sea surface temperature (SST) and salinity (SSS) respond to the increased freshwater and latent heat fluxes (Figures 13 and 14). The SST and SSS responses were similar in winter and summer, so presented responses include data from all seasons.

Strong surface cooling and freshening of Antarctic waters is expected in all the experiments, as the meltwater remains at the surface (Figure 16a), cooling and enhancing stratification (although Antarctic coastal waters are likely to be at, or close to, freezing and cannot be cooled further). The SST and SSS anomalies may be distributed differently in the experiments, as some of the anomaly is the direct effect of the additional melt, and some is the result of the increased sea ice volume stimulated by the additional melt. The Southern Ocean surface freshens in all experiments, but the freshening is slightly stronger in FWShelf than in FWBerg along the Antarctic coast, reflecting large ice shelf melt fluxes. Freshening is slightly stronger in FWBerg north east of the Antarctic Peninsula, where iceberg melt is high (Figure 2). The strongest surface cooling occurs in FWShelf, which represents the most spatially concentrated additional melt flux, and is weakest in FWBerg, where the melt is most widely distributed. Surface cooling in FW is somewhere between FWShelf and FWBerg as expected. Surface waters around New Zealand, Southern Australia, South America and the southern tip of Africa freshen in all the experiments, with a similar spatial distribution for the salinity response in FWShelf and FWBerg, although the magnitude of the anomalies is greater in FWShelf than in FWBerg. FWShelf also results in greater cooling at latitudes far from Antarctica than FWBerg, meaning that the distal effects in Figures 14 and 13 for FW cannot be attributed to melt from far-travelling icebergs, but is more likely to be associated with the processes discussed below. Both FWShelf and FWBerg result in stronger surface salinity anomalies in the northern hemisphere than are seen in FW, suggesting some interdependency of responses to the two processes.

There is a strong increase in SSS in the Arctic Ocean in all the experiments, which cannot be explained by saltier water upwelling since there is no deepening of the mixed layer (Figure S3 in Supplemental Material), or by changes to the relative river discharge rates into the different ocean basins (Figure S4 in Supplemental Material). The SSS response here and throughout the northern hemisphere agrees with that in van den Berk et al. (2019), where increasing meltwater fluxes around Antarctica resulted in changes to ocean circulation that impacted on salt transport into (and out of) the Arctic Ocean over a similar timescale to our experiments, using a similar model. The mechanisms shown in that work to link an Antarctic meltwater perturbation to SSS changes in the North Atlantic are complex, and we refer the reader to van den Berk et al. (2019) for a comprehensive description. Alternative oceanic mechanisms were proposed to explain similar northern hemisphere anomalies in response to an Antarctic freshwater perturbation in Richardson et al. (2005). Further work using our results would be a useful verification of those studies but is beyond the scope of the present study. Nonetheless, our findings support the assertion that the effects of Antarctic meltwater fluxes on northern hemisphere ocean circulation are significant, possibly more so than Arctic meltwater effects since Antarctica represents a much larger freshwater source (van den Berk et al. 2019), and because the surface salinity response does not remain local to the Antarctic meltwater perturbation location (in contrast to Arctic meltwater perturbations (Ronald et al. 2007)).

Density and Temperature

By the end of the experiments, upper ocean waters closest to the source of the melt perturbation have become less dense due to freshening, while those further north have become more dense due to cooling (density is calculated relative to 2000 m using the UNESCO Equation of State (Jackett and Mcdougall 1995)) (Figures 15, 16, 17). In all the experiments, freshening at high latitudes decreases the water density from the surface to the depth of the continental shelf. The anomaly is strongest in FWShelf and FW, where the freshening from ice shelf melt spans the depths of the ice shelf drafts, but it is also apparent in FWBerg, where iceberg melt enters the surface ocean. Although stratification is enhanced in FWBerg, convection driven by brine rejection continues to mix the iceberg melt with the underlying waters in some areas, creating the weak freshening and positive density anomaly that extends to the continental shelf depth at high latitudes.

Mid-layer waters warm near the Antarctic coast in all three experiments. This is because the increased sea ice cover and the fresher, more buoyant overlying waters prevent mid-layer water from rising and exchanging heat with the atmosphere. This warming is strongest in FW and FWShelf, for which the freshening of the coastal waters is strongest because of the ice shelf melt flux, and surface cooling north of the sea ice edge is strongest. In FWShelf, the warm anomaly in Figure 15c extends north and reaches to the sea floor at mid-latitudes, reflecting the reduction in AABW driven by the freshening effect of the ice shelf melt (Figure 11). The warm signal also extends to the mid-latitudes in FW (Figure 15b), although it remains further south, and is mostly confined to the upper layers of the water affected by the warming in FWShelf. In FWBerg, where AABW is largely unchanged from PIControl (Figure 11), the warm anomaly does not extend to the sea floor beyond the continental shelf edge, and is confined to the sea ice region (Figure 15d). Similar warming of mid-layer waters was found by Bronselaer et al. (2018), where it was explained by increased stratification that prevented these waters from mixing with surface waters and cooling as they travelled polewards. This increased the heat transported to the coast, potentially contributing to a reduction in AABW formation in that study.

In our study, the mixed layer becomes shallower north of the sea ice region in response to both ice shelf and iceberg melt (Figure 10). If the warming of mid-latitude waters were solely driven by increased stratification, then we would expect mid-latitude waters in FWBerg to warm similarly to the same waters in FWShelf and FW, although more weakly since the stratification is slightly weaker (Figure 10). However, the warming of deeper waters beyond the sea ice region occurs only in FW and FWShelf (Figure15), so cannot be completely driven by the increased stratification. The freshening of the water column above the continental shelf reduces AABW formation in FWShelf and FW (Figure 11), and the warm anomaly that spreads down to the shelf and over the shelf edge in Figures 15b and 15c is due to reduced cold AABW production in FWShelf and FW, compared to PIControl. AABW formation in FWBerg is similar to PIControl (Figure 11), and therefore there is no deeper warm anomaly in FWBerg, relative to PIControl. The reduction in AABW production in FWShelf and FW creates a warm anomaly in deeper mid-latitude waters, which may then allow for increased heat transport to the coast, further reducing AABW formation.

Surface cooling becomes stronger north of the sea ice edge in all the experiments. The cooling, and resultant density increase, is confined to increasingly shallow depths as the signal extends north. The cooling and density increase of upper ocean waters far from the coast is weakest in FWBerg, despite melt in this experiment being distributed over the widest range of latitudes. This may be because the local changes to ocean volume and salinity that are responsible for the ocean circulation effects identified in van den Berk et al. (2019) (see Section 3) are stronger in FWShelf, where the increasing freshwater flux is more spatially concentrated. For all the experiments, the high latitude decrease in surface density is greater than the lower latitude increase, reflecting a reduction in the meridional density gradient which could impact on the Antarctic Circumpolar Current (Russell et al. 2006).

Antarctic Circumpolar Current (ACC)

The ACC is a central component of global ocean circulation, linking the subtropical and subpolar gyres and providing a barrier to heat transport from lower latitudes to the polar region. It weakens over the course of all the experiments following the decreased meridional density gradient (Figure 18).

Following Russell et al. (2006), we consider both the ACC and the difference in the upper ocean density between 65° S and 45° S that is associated with the eastward geostrophic flow, to confirm that the ACC declines as the meridional density difference reduces (Figure 19). The greatest reduction in the ACC, and the closest relationship between this and the density difference, occurs in FWShelf, where the density gradient has experienced the greatest decrease. To determine whether salinity or temperature provide the primary driver for the density gradient changes, we again follow Russell et al. (2006) and consider the evolution of the difference in zonally-averaged upper ocean density, temperature and salinity at the two latitudes (Figure 20). The density difference closely follows the temperature difference (rather than the salinity difference) in all the experiments (only FW shown).

An increasing melt flux entering Antarctic coastal waters reduces the meridional density gradient across the Southern Ocean by impacting on near surface temperature, and, to a lesser extent, on near surface salinity. This causes a reduction in ACC transport. The ACC is much less sensitive to iceberg melt, which enters the ocean distributed across a wider range of latitudes, than to melt from ice shelves.

Wind Stress

The cold atmosphere at high latitudes creates a meridional gradient in the surface heat flux (the heat exchanged between the ocean and atmosphere), which is one factor that drives the westerly jet associated with the SAM (Kidston et al. 2011). In the experiments, cooler surface temperatures and increased sea ice cover reduce the surface heat flux, and so potentially impact the jet, particularly in winter, when the sea ice extends further north and the changes to the surface heat flux therefore occur closer to the jet's peak (the jet is more sensitive to changes in the vicinity of the peak wind (Kidston et al. 2011)). In our experiments, this results in August, September, October being the period with the strongest wind response, in agreement with other studies (Kidston et al. 2011; Bader et al. 2013; Grise and Polvani 2016) (the maximum sea ice extent occurs in September (Figure 3)). We define the maximum zonally averaged westerly wind stress on the ocean surface as a proxy for the jet strength, and take the latitude at which this occurs as the jet position (Figure 21).

Changes to the peak wind strength and position may be small relative to the model grid resolution, and so the peak wind strength and position were read from a curve fitted around the three grid points centred on the maximum wind stress in Figure 21. Figure 22 shows the evolution of the peak strength through the simulations. The peak position and strength for the experiments were compared to those for PIControl over the final 20 years of each simulation using a student t-test to assess the significance of any change to the mean (Table 2). We found no change to the latitude of the peak wind stress, in agreement with Bracegirdle et al. (2018), who found no strong relationship between sea ice area and jet location. There was a small change in the strength of the peak wind stress by the end of FW (0.019 Nm^{-2}), significant at the 95% confidence level, and a similar change (0.016 Nm^{-2}) by the end of FWShelf, significant at the 90% confidence level.

There was no significant change in wind strength by the end of FWBerg. The changes in strength are small, but suggest that the westerly winds may strengthen in response to increased sea ice cover, supporting the relationship between sea ice area and jet strength suggested in other works, e.g., Menéndez et al. (1999); Kidston et al. (2011); Bader et al. (2013); Grise and Polvani (2016); Bracegirdle et al. (2018). However, the fact that there is no significant strengthening in FWBerg, which corresponds to only slightly smaller changes in sea ice cover than FW and FWShelf (Figures 7), suggests that either a very large increase in sea ice area is required to impact the westerly winds, or that some other response to ice shelf melt (but not to iceberg melt) drives the wind response. Surface cooling at high latitudes impacts the surface heat flux similarly to sea ice cover, and so drives a similar wind response. The surface cooling at the latitudes surrounding the peak wind stress (approximately 45 - 55° S (Figure 21)) is much greater in FW and FWShelf than in FWBerg (Figure 13), and so results in a strengthening of the wind that is absent in FWBerg. The westerly jet extends into the atmosphere and is subject to other atmospheric effects which may impact on the stress experienced at the surface. Such effects may be stronger than the effect of sea ice and surface temperature changes, and further work to analyse these, and the influence of the increasing meltwater on them, is needed but is beyond the scope of this work.

Precipitation

Precipitation minus evaporation (P - E) is the greatest freshwater contribution to the ocean south of 50° S (Figure S5 in Supplemental Material). In the model, rainfall onto sea ice is assumed to run off, but snowfall onto sea ice is transported northwards to where the sea ice melts. An increase in sea ice area reduces the amount of precipitation reaching the ocean (Figure 23a). The decrease is greater than the reduction in evaporation, and so P-E decreases (Figure 23b). This salinification opposes the freshening effect of the increasing meltwater fluxes at high latitudes but does not extend beyond the latitudes of increased sea ice cover (not shown).

Increased sea ice cover and ocean stratification insulate the surface ocean, reducing the surface heat flux and cooling the lower atmosphere, making precipitation more likely to be snow, and reducing evaporation. Snow melts on entering the ocean, absorbing latent heat to cool the ocean in a way that rain does not. Although the total snowfall entering the ocean does not increase in the experiments, there is a northwards shift of the polar front (the boundary between the air masses of the polar cell and the Ferrell cell), where the dominant form of precipitation switches between snow and rain (Figure 23c). This means that the cooling effect of snow on the surface ocean has shifted northwards in response to the increased melt fluxes, enhancing the surface cooling that is driven directly by the increased freshwater flux (Figure 13). Previous studies have also shown that a freshwater perturbation at high southern latitudes shifts the intertropical convergence zone (ITCZ) northwards, resulting in shifted tropical precipitation patterns (Bronselaer et al. 2018). This mainly follows from the cooling in the southern hemisphere, which drives a compensating increase in the southward atmospheric heat flux, and results from all our experiments concur with this (Figure 24) (only the anomaly from FW is shown).

Summary and Discussion

Antarctic sea ice expands and thickens in response to an increasing meltwater flux, with regional variations in the response that are mostly explained by the transport of meltwater and icebergs by the ocean circulation. The response to increasing ice shelf melt is faster and stronger than that for increasing iceberg melt because all meltwater enters the ocean within the sea ice formation region, but otherwise the sea ice response is similar for increasing meltwater fluxes from both sources (notwithstanding regional differences attributable to the accessibility of some areas to icebergs). This agrees with previous studies (e.g., Pauling et al. (2016)), however here we have identified which sea ice growth processes are enhanced by the increasing freshwater input, and assessed the sensitivities of these to the different meltwater sources. We find that sea ice growth is enhanced by surface cooling which inhibits basal melt, and as the ice thickens in response to this, the basal temperature becomes less conducive to congelation growth, and so frazil growth accounts for a greater proportion of total sea ice growth. Ice shelf melt entering the ocean at depth constitutes a source of supercooling, increasing frazil production, which becomes the dominant mechanism for sea ice growth when ice shelf melt is present. While we find that meltwater from both ice shelves and icebergs drives a similar increase in sea ice growth, the effect of iceberg melt is to enhance stratification in agreement with Pauling et al. (2016). Our results show that as ice shelf melt increases, the rising buoyant meltwater drives a local overturning which deepens the mixed layer. This response to increasing ice shelf melt encourages the formation of shore leads, as shown by Jourdain et al. (2017); Merino et al. (2018). We show that the response to iceberg melt contrasts with this as the increased stratification drives in-situ freezing of sea ice at the coast. We have also shown that the increased stratification induced by iceberg melt can counter increases in AABW formation that may ordinarily be associated with increased sea ice formation, and that the reduction in AABW formation that follows from large ice shelf meltwater fluxes is the result of a different process, i.e., the freshening of the water column. This demonstrates circumstances where increased sea ice production does not lead to increased AABW formation. AABW is a driver for the thermohaline circulation (Marsland et al. 2007), and inappropriate representation of formation rates through inappropriate representation of meltwater fluxes is therefore likely to result in an unrealistic representation of the thermohaline circulation, and therefore also of global oceanic heat transport and its response to climate change.

The ocean surface cools and mid-layer waters warm in response to increases in both ice shelf and iceberg melt, in agreement with Pauling et al. (2016); Bronselaer et al. (2018), however our results show that the warming response extends further north and to greater depths for increasing ice shelf melt. We find near-surface density changes that agree with the response to Antarctic meltwater-induced circulation changes in van den Berk et al. (2019), even far from the perturbation source, and we show that these changes are more sensitive to increased, concentrated meltwater anomalies at depth than to distributed melt at the surface. We demonstrate that, as a more concentrated meltwater source, increasing ice shelf melt has a greater impact on the meridional density gradient than increasing iceberg melt, and therefore drives a more severe decrease in ACC transport. These differences highlight the importance of appropriately representing these two separate melt pathways in climate studies to ensure that projections capture the likely future climate.

We find a small strengthening of the westerly circumpolar winds in response to the increased meltwater fluxes in agreement with Menéndez et al. (1999); Kidston et al. (2011); Bader et al. (2013); Grise and Polvani (2016); Bracegirdle et al. (2018). However, in contrast to most previous works, we suggest this may be partially driven by cooling of the ocean surface, in addition to the increased sea ice extent. We found no change to the latitude of the peak wind strength, in agreement with Bracegirdle et al. (2018). As shown in previous studies (e.g., Bronselaer et al. (2018)), we find increasing the rate at which Antarctic meltwater fluxes enter the Southern Ocean causes the meteorological polar front to shift northwards, meaning that latent heat cooling from snowfall affects the ocean at lower latitudes and the ITCZ shifts north. Our results include significant effects on ocean SST and SSS that extend into the northern hemisphere and cannot be explained by far-travelling icebergs. Neglecting the increasing melt rate of Antarctica could therefore have implications for projections of northern hemisphere climate. Some research into the mechanisms that drive these distal effects exists (Richardson et al. 2005; Ronald et al. 2007; van den Berk et al. 2019), but more is needed so that we can understand the implications of increasing Antarctic meltwater fluxes for the wider northern hemisphere climate system.

The model used here includes improvements to the representation of ice shelf and iceberg meltwater fluxes in a fully coupled climate model compared to CMIP5 generation models, but there remain some simplifications that may impact on the presented sensitivities. For example, small icebergs account for most of the iceberg meltwater flux into the Southern Ocean (Tournadre et al. 2015), but larger icebergs do occur, and these follow different trajectories, persist for longer and melt with less seasonal dependence (since their keels extend into deeper ocean layers where seasonal temperature variability is less), creating temporally and spatially local peaks in the iceberg meltwater flux that are not captured in HadGEM3-GC3.1 (Rackow et al. 2017). In particular, larger icebergs may persist for longer in the Antarctic coastal current and provide a more persistent, distributed meltwater source at the coast than simulated in our study (Silva et al. 2006; Rackow et al. 2017). Icebergs extend below the ocean surface and interact with subsurface ocean currents, meaning their trajectories, and the spatial distribution of the melt-induced cooling effect, may differ from our simulations. Similarly, iceberg melt rates may not always be realistically represented since water temperature at the iceberg base is unlikely to always differ from the surface temperature by 4° C (although most melt from icebergs surrounded by ocean is attributable to wave erosion rather than to basal melt (Marsh et al. 2015)). Improvements to iceberg representation have been implemented in stand-alone and coupled ocean-sea ice models, allowing for large tabular icebergs and for dynamic coupling with subsurface ocean properties (Merino et al. 2016; Stern et al. 2017; Marson et al. 2018). Including these developments in future fully coupled (atmosphere-ocean-sea ice) climate models will make simulated iceberg meltwater fluxes more realistic. Representing open ice shelf cavities in a coupled climate model remains a challenge, however the new parametrization implemented here approximates the cavity more realistically than was previously possible in coupled climate models Mathiot et al. (2017), and the resulting meltwater distribution is thought to be realistic, giving us confidence in the presented sensitivities. For this sensitivity study, all other external forcings were fixed at pre-industrial levels, however some of the responses presented here may be countered by the effects of increasing greenhouse gas emissions in a more realistic environment, and this is an active area of research (Mackie et al. submitted). Future model development will allow dynamic coupling of an ice sheet model to the climate model. The sensitivities found here demonstrate the importance of that work, which will allow climate projections to be calculated accounting for realistically increasing meltwater fluxes from ice shelves and icebergs. Current climate projections that do not account for increasing Antarctic melt rates, or for separate iceberg and ice shelf melt sources and their different effects, should be interpreted in light of the sensitivities presented here.

Acknowledgments. This work was funded by New Zealand Deep South National Science Challenge, MBIE contract C01X142. Data for PIControl were calculated by the Hadley Centre, U.K. Met Office for submission to the CMIP6 experiment. The project is grateful for support from Professor Bitz at University of Washington. We acknowledge use of the Monsoon2 system, and the High Capacity Storage Service at University of Otago, New Zealand. Model data analysed in this work are publicly available at Mackie et al. (2020).

References

Bader, J., M. Flügge, N. G. Kvamstø, M. D. S. Mesquita, and A. Voigt, 2013: Atmospheric winter response to a projected future Antarctic sea-ice reduction: a dynamical analysis. *Climate Dynamics*, **40 (11)**, 2707–2718, doi:10.1007/s00382-012-1507-9.

Bigg, G. R., M. R. Wadley, D. P. Stevens, and J. A. Johnson, 1997: Modelling the dynamics and thermodynamics of icebergs. *Cold Regions Science and Technology*, **26 (2)**, 113 – 135, doi:https://doi.org/10.1016/S0165-232X(97)00012-8.

Bintanja, R., G. van Oldenborgh, and C. Katsman, 2015: The effect of increased fresh water from Antarctic ice shelves on future trends in Antarctic sea ice. *Annals of Glaciology*, **56 (69)**, 120126, doi:10.3189/2015AoG69A001.

Bintanja, R., G. J. van Oldenborgh, S. S. Drijfhout, B. Wouters, and C. A. Katsman, 2013: Important role for ocean warming and increased ice-shelf melt in Antarctic sea-ice expansion. *Nature Geoscience*, **6**, 376 EP –, URL http://dx.doi.org/10.1038/ngeo1767.

Bracegirdle, T. J., P. Hyder, and C. R. Holmes, 2018: CMIP5 diversity in southern westerly jet projections related to historical sea ice area: Strong link to strengthening and weak link to shift. *Journal of Climate*, **31 (1)**, 195–211, doi:10.1175/JCLI-D-17-0320.1.

Bracegirdle, T. J., E. Shuckburgh, J.-B. Sallee, Z. Wang, A. J. S. Meijers, N. Bruneau, T. Phillips, and L. J. Wilcox, 2013: Assessment of surface winds over the Atlantic, Indian, and Pacific Ocean sectors of the Southern Ocean in CMIP5 models: historical bias, forcing response, and state dependence. *Journal of Geophysical Research: Atmospheres*, **118 (2)**, 547–562, doi:10.1002/jgrd.50153.

Bronselaer, B., M. Winton, S. M. Griffies, W. J. Hurlin, K. B. Rodgers, O. V. Sergienko, R. J. Stouffer, and J. L. Russell, 2018: Change in future climate due to Antarctic meltwater. *Nature*, doi:10.1038/s41586-018-0712-z.

Buckley, M. W., and J. Marshall, 2016: Observations, inferences, and mechanisms of the Atlantic Meridional Overturning Circulation: A review. *Reviews of Geophysics*, **54 (1)**, 5–63, doi:10.

1002/2015RG000493.

Cavalieri, D. J., and C. L. Parkinson, 2008: Antarctic sea ice variability and trends, 19792006. *Journal of Geophysical Research: Oceans*, **113 (C7)**, doi:10.1029/2007JC004564.

Comiso, J. C., R. Kwok, S. Martin, and A. L. Gordon, 2011: Variability and trends in sea ice extent and ice production in the Ross Sea. *Journal of Geophysical Research: Oceans*, **116 (C4)**, doi:10.1029/2010JC006391.

DeConto, R. M., and D. Pollard, 2016: Contribution of Antarctica to past and future sea-level rise. *Nature*, **531**, 591 EP –, article.

Depoorter, M. A., J. L. Bamber, J. A. Griggs, J. T. M. Lenaerts, S. R. M. Ligtenberg, M. R. van den Broeke, and G. Moholdt, 2013: Calving fluxes and basal melt rates of Antarctic ice shelves. *Nature*, **502**, 89 EP –, doi:10.1038/nature12567.

Grise, K. M., and L. M. Polvani, 2016: Is climate sensitivity related to dynamical sensitivity? *Journal of Geophysical Research: Atmospheres*, **121 (10)**, 5159–5176, doi:10.1002/2015JD024687.

Hellmer, H. H., 2004: Impact of Antarctic ice shelf basal melting on sea ice and deep ocean properties. *Geophysical Research Letters*, **31 (10)**, doi:10.1029/2004GL019506.

Heuzé, C., K. J. Heywood, D. P. Stevens, and J. K. Ridley, 2015: Changes in global ocean bottom properties and volume transports in CMIP5 models under climate change scenarios. *Journal of Climate*, **28 (8)**, 2917–2944, doi:10.1175/JCLI-D-14-00381.1.

Hoskins, B. J., and K. I. Hodges, 2005: A new perspective on southern hemisphere storm tracks. *Journal of Climate*, **18 (20)**, 4108–4129, doi:10.1175/JCLI3570.1, URL https://doi.org/10.1175/JCLI3570.1, https://doi.org/10.1175/JCLI3570.1.

Hunke, E. C., W. H. Lipscomb, A. K. Turner, N. Jeffrey, and S. Elliott, 2015: CICE: the Los Alamos sea ice model documentation and software users manual version 5.1, LA-CC-06-012. Tech. rep., Los Alamos National Laboratory, Los Alamos NM 87545.

Jackett, D. R., and T. J. Mcdougall, 1995: Minimal adjustment of hydrographic profiles to achieve static stability. *Journal of Atmospheric and Oceanic Technology*, **12 (2)**, 381–389, doi:10.1175/1520-0426(1995)012⟨0381:MAOHPT⟩2.0.CO;2.

Jourdain, N. C., P. Mathiot, N. Merino, G. Durand, J. Le Sommer, P. Spence, P. Dutrieux, and G. Madec, 2017: Ocean circulation and sea-ice thinning induced by melting ice shelves in the Amundsen Sea. *Journal of Geophysical Research: Oceans*, **122 (3)**, 2550–2573, doi:10.1002/2016JC012509.

Kidston, J., A. S. Taschetto, D. W. J. Thompson, and M. H. England, 2011: The influence of southern hemisphere sea-ice extent on the latitude of the mid-latitude jet stream. *Geophysical Research Letters*, **38 (15)**, doi:10.1029/2011GL048056.

Kuhlbrodt, T., and Coauthors, 2018: The lowresolution version of HadGEM3 GC3.1: Development and evaluation for global climate. *Journal of Advances in Modeling Earth Systems*, doi:10.1029/2018MS001370.

Lago, V., and M. H. England, 2019: Projected slowdown of Antarctic Bottom Water formation in response to amplified meltwater contributions. *Journal of Climate*, **32 (19)**, 6319–6335, doi:10.1175/JCLI-D-18-0622.1.

Langhorne, P. J., and Coauthors, 2015: Observed platelet ice distributions in Antarctic sea ice: An index for ocean-ice shelf heat flux. *Geophysical Research Letters*, **42 (13)**, 5442–5451, doi:10.1002/2015GL064508.

Le Quéré, C., and Coauthors, 2007: Saturation of the Southern Ocean CO2 sink due to recent climate change. *Science*, **316 (5832)**, 1735–1738, doi:10.1126/science.1136188.

Liston, G. E., and J.-G. Winther, 2005: Antarctic surface and subsurface snow and ice melt fluxes. *Journal of Climate*, **18 (10)**, 1469–1481, doi:10.1175/JCLI3344.1.

Losch, M., 2008: Modeling ice shelf cavities in a z coordinate ocean general circulation model. *Journal of Geophysical Research: Oceans*, **113 (C8)**, doi:10.1029/2007JC004368.

M. van Aken, H., 2007: *The Oceanic Thermohaline Circulation: An Introduction*, Atmospheric and Oceanographic Sciences Library, Vol. 39. Springer-Verlag, New York, doi:10.1007/978-0-387-48039-8.

Mackie, S., I. J. Smith, J. K. Ridley, D. P. Stevens, and P. J. Langhorne, 2020: Climate model response to increasing Antarctic iceberg and ice shelf melt. PANGAEA, URL https://doi.org/10.1594/PANGAEA.911392, doi:10.1594/PANGAEA.911392.

Mackie, S., I. J. Smith, D. P. Stevens, J. K. Ridley, and P. J. Langhorne, submitted: Interactions between increasing CO_2 and Antarctic melt rates. *Journal of Climate*, **this issue**.

Madec, G., and N. team, 2016: NEMO ocean engine, version 3.6 stable. Tech. rep., Pole de modelisation de lInstitut Pierre-Simon Laplace.

Marsh, R., and Coauthors, 2015: NEMO-ICB (v1.0): interactive icebergs in the NEMO ocean model globally configured at eddy-permitting resolution. *Geoscientific Model Development*, **8 (5)**, 1547–1562, doi:10.5194/gmd-8-1547-2015.

Marsland, S. J., J. A. Church, N. L. Bindoff, and G. D. Williams, 2007: Antarctic coastal polynya response to climate change. *Journal of Geophysical Research: Oceans*, **112 (C7)**, doi:10.1029/2005JC003291.

Marson, J. M., P. G. Myers, X. Hu, and J. Le Sommer, 2018: Using vertically integrated ocean fields to characterize Greenland icebergs' distribution and lifetime. *Geophysical Research Letters*, **45 (9)**, 4208–4217, doi:10.1029/2018GL077676.

Martin, T., and A. Adcroft, 2010: Parameterizing the fresh-water flux from land ice to ocean with interactive icebergs in a coupled climate model. *Ocean Modelling*, **34 (3)**, 111–124, doi: https://doi.org/10.1016/j.ocemod.2010.05.001.

Martin-Espanol, A., and Coauthors, 2016: Spatial and temporal Antarctic Ice Sheet mass trends, glacio-isostatic adjustment, and surface processes from a joint inversion of satellite altimeter, gravity, and GPS data. *Journal of Geophysical Research: Earth Surface*, **121 (2)**, 182–200.

Mathiot, P., A. Jenkins, C. Harris, and G. Madec, 2017: Explicit representation and parametrised impacts of under ice shelf seas in the z^* coordinate ocean model NEMO 3.6. *Geoscientific Model Development*, **10 (7)**, 2849–2874, doi:10.5194/gmd-10-2849-2017.

Menéndez, C. G., V. Serafini, and H. Le Treut, 1999: The effect of sea-ice on the transient atmospheric eddies of the Southern Hemisphere. *Climate Dynamics*, **15 (9)**, 659–671, doi: 10.1007/s003820050308.

Merino, N., N. C. Jourdain, J. L. Sommer, H. Goosse, P. Mathiot, and G. Durand, 2018: Impact of increasing Antarctic glacial freshwater release on regional sea-ice cover in the Southern Ocean. *Ocean Modelling*, **121**, 76 – 89, doi:https://doi.org/10.1016/j.ocemod.2017.11.009.

Merino, N., J. L. Sommer, G. Durand, N. C. Jourdain, G. Madec, P. Mathiot, and J. Tournadre, 2016: Antarctic icebergs melt over the Southern Ocean: Climatology and impact on sea ice. *Ocean Modelling*, **104**, 99 – 110, doi:https://doi.org/10.1016/j.ocemod.2016.05.001.

Morrison, A. K., M. H. England, and A. M. Hogg, 2015: Response of Southern Ocean convection and abyssal overturning to surface buoyancy perturbations. *Journal of Climate*, **28 (10)**, 4263–4278, doi:10.1175/JCLI-D-14-00110.1.

Nicholls, K. W., S. sterhus, K. Makinson, T. Gammelsrd, and E. Fahrbach, 2009: Ice-ocean processes over the continental shelf of the southern Weddell Sea, Antarctica: A review. *Reviews of Geophysics*, **47 (3)**, doi:10.1029/2007RG000250.

Paolo, F. S., H. A. Fricker, and L. Padman, 2015: Volume loss from Antarctic ice shelves is accelerating. *Science*, **348 (6232)**, 327–331, doi:10.1126/science.aaa0940.

Parkinson, C. L., 2019: A 40-y record reveals gradual Antarctic sea ice increases followed by decreases at rates far exceeding the rates seen in the Arctic. *Proceedings of the National Academy of Sciences*, **116 (29)**, 14 414–14 423, doi:10.1073/pnas.1906556116.

Pauling, A. G., C. M. Bitz, I. J. Smith, and P. J. Langhorne, 2016: The response of the Southern Ocean and Antarctic sea ice to freshwater from ice shelves in an Earth System Model. *Journal of Climate*, 1655–1672.

Pauling, A. G., I. J. Smith, P. J. Langhorne, and C. M. Bitz, 2017: Time-dependent freshwater input from ice shelves: Impacts on Antarctic sea ice and the Southern Ocean in an Earth System Model. *Geophysical Research Letters*, **44 (20)**, 10,454–10,461, doi:10.1002/2017GL075017.

Pezza, A. B., H. A. Rashid, and I. Simmonds, 2012: Climate links and recent extremes in antarctic sea ice, high-latitude cyclones, southern annular mode and enso. *Climate Dynamics*, **38 (1)**, 57–73, doi:10.1007/s00382-011-1044-y, URL https://doi.org/10.1007/s00382-011-1044-y.

Purich, A., M. H. England, W. Cai, A. Sullivan, and P. J. Durack, 2018: Impacts of broad-scale surface freshening of the Southern Ocean in a coupled climate model. *Journal of Climate*, **31 (7)**, 2613–2632, doi:10.1175/JCLI-D-17-0092.1.

Rackow, T., C. Wesche, R. Timmermann, H. H. Hellmer, S. Juricke, and T. Jung, 2017: A simulation of small to giant Antarctic iceberg evolution: Differential impact on climatology estimates. *Journal of Geophysical Research: Oceans*, **122 (4)**, 3170–3190, doi:10.1002/2016JC012513.

Rahmstorf, S., J. E. Box, G. Feulner, M. E. Mann, A. Robinson, S. Rutherford, and E. J. Schaffernicht, 2015: Exceptional twentieth-century slowdown in Atlantic Ocean overturning circulation. *Nature Climate Change*, **5**, 475 EP –, article.

Richardson, G., M. R. Wadley, K. J. Heywood, D. P. Stevens, and H. T. Banks, 2005: Short-term climate response to a freshwater pulse in the Southern Ocean. *Geophysical Research Letters*, **32 (3)**, doi:10.1029/2004GL021586.

Ridley, J. K., E. W. Blockley, A. B. Keen, J. G. L. Rae, A. E. West, and D. Schroeder, 2018: The sea ice model component of HadGEM3-GC3.1. *Geoscientific Model Development*, **11 (2)**, 713–723, doi:10.5194/gmd-11-713-2018.

Rignot, E., J. L. Bamber, M. R. van den Broeke, C. Davis, Y. Li, W. J. van de Berg, and E. van Meijgaard, 2008: Recent Antarctic ice mass loss from radar interferometry and regional climate modelling. *Nature Geoscience*, **1**, 106 EP –.

Rignot, E., S. Jacobs, J. Mouginot, and B. Scheuchl, 2013: Ice-shelf melting around Antarctica. *Science*, **341 (6143)**, 266–270, doi:10.1126/science.1235798.

Ronald, S., D. Seidov, and B. Haupt, 2007: Climate response to external sources of freshwater: North Atlantic versus the Southern Ocean. *Journal of Climate*, **20**, 436–448.

Russell, J. L., R. J. Stouffer, and K. W. Dixon, 2006: Intercomparison of the Southern Ocean circulations in IPCC coupled model control simulations. *Journal of Climate*, **19 (18)**, 4560–4575, doi:10.1175/JCLI3869.1.

Schloesser, F., T. Friedrich, A. Timmermann, R. M. DeConto, and D. Pollard, 2019: Antarctic iceberg impacts on future Southern Hemisphere climate. *Nature Climate Change*, **9 (9)**, 672–677, doi:10.1038/s41558-019-0546-1.

Sévellec, F., and A. V. Fedorov, 2016: AMOC sensitivity to surface buoyancy fluxes: Stronger ocean meridional heat transport with a weaker volume transport? *Climate Dynamics*, **47 (5)**, 1497–1513, doi:10.1007/s00382-015-2915-4.

Shepherd, A., and Coauthors, 2018: Mass balance of the Antarctic Ice Sheet from 1992 to 2017. *Nature*, **558 (7709)**, 219–222, doi:10.1038/s41586-018-0179-y.

Silva, T. A. M., G. R. Bigg, and K. W. Nicholls, 2006: Contribution of giant icebergs to the Southern Ocean freshwater flux. *Journal of Geophysical Research: Oceans*, **111 (C3)**, doi:10.1029/2004JC002843.

Silvano, A., S. R. Rintoul, B. Peña-Molino, W. R. Hobbs, E. van Wijk, S. Aoki, T. Tamura, and G. D. Williams, 2018: Freshening by glacial meltwater enhances melting of ice shelves and reduces formation of Antarctic Bottom Water. *Science Advances*, **4 (4)**, doi:10.1126/sciadv.aap9467.

Sloyan, B. M., 2006: Antarctic bottom and lower circumpolar deep water circulation in the eastern Indian Ocean. *Journal of Geophysical Research: Oceans*, **111 (C2)**, doi:10.1029/2005JC003011.

Smith, I., P. Langhorne, R. Frew, R. Vennell, and T. Haskell, 2012: Sea ice growth rates near ice shelves. *Cold Regions Science and Technology*, **83-84**, 57 – 70, doi:https://doi.org/10.1016/j.coldregions.2012.06.005.

Smith, I. J., P. J. Langhorne, T. G. Haskell, H. Joe Trodahl, R. Frew, and M. Ross Vennell, 2001: Platelet ice and the land-fast sea ice of McMurdo Sound, Antarctica. *Annals of Glaciology*, **33**, 2127, doi:10.3189/172756401781818365.

Stammerjohn, S. E., D. G. Martinson, R. C. Smith, X. Yuan, and D. Rind, 2008: Trends in Antarctic annual sea ice retreat and advance and their relation to El NioSouthern Oscillation and Southern Annular Mode variability. *Journal of Geophysical Research: Oceans*, **113 (C3)**, doi:10.1029/2007JC004269.

Stern, A. A., A. Adcroft, O. Sergienko, and G. Marques, 2017: Modeling tabular icebergs submerged in the ocean. *Journal of Advances in Modeling Earth Systems*, **9 (4)**, 1948–1972, doi:10.1002/2017MS001002.

Storkey, D., and Coauthors, 2018: UK Global Ocean GO6 and GO7: a traceable hierarchy of model resolutions. *Geoscientific Model Development*, **11 (8)**, 3187–3213, doi:10.5194/gmd-11-3187-2018.

Sutterley, T. C., I. Velicogna, E. Rignot, J. Mouginot, T. Flament, M. R. Van Den Broeke, J. M. Van Wessem, and C. H. Reijmer, 2014: Mass loss of the Amundsen Sea Embayment of West Antarctica from four independent techniques. *Geophysical Research Letters*, **41 (23)**, 8421–8428.

Swart, N. C., and J. C. Fyfe, 2013: The influence of recent Antarctic ice sheet retreat on simulated sea ice area trends. *Geophysical Research Letters*, **40**, 4328–4332.

Timmermann, R., and H. H. Hellmer, 2013: Southern Ocean warming and increased ice shelf basal melting in the twenty-first and twenty-second centuries based on coupled ice-ocean finite-element modelling. *Ocean Dynamics*, **63 (9)**, 1011–1026, doi:10.1007/s10236-013-0642-0.

Tournadre, J., N. Bouhier, F. Girard-Ardhuin, and F. Rémy, 2015: Large icebergs characteristics from altimeter waveforms analysis. *Journal of Geophysical Research: Oceans*, **120 (3)**, 1954–1974, doi:10.1002/2014JC010502.

Turner, J., T. J. Bracegirdle, T. Phillips, G. J. Marshall, and J. S. Hosking, 2013: An initial assessment of Antarctic sea ice extent in the CMIP5 models. *Journal of Climate*, **26 (5)**, 1473–1484, doi:10.1175/JCLI-D-12-00068.1.

Turner, J., and Coauthors, 2009: Non-annular atmospheric circulation change induced by stratospheric ozone depletion and its role in the recent increase of Antarctic sea ice extent. *Geophysical Research Letters*, **36 (8)**, doi:10.1029/2009GL037524.

van den Berk, J., S. S. Drijfhout, and W. Hazeleger, 2019: Atlantic salinity budget in response to Northern and Southern Hemisphere ice sheet discharge. *Climate Dynamics*, **52 (9)**, 5249–5267, doi:10.1007/s00382-018-4444-4.

Weaver, A. J., O. A. Saenko, P. U. Clark, and J. X. Mitrovica, 2003: Meltwater Pulse 1A from Antarctica as a trigger of the Bølling-Allerød Warm Interval. *Science*, **299 (5613)**, 1709–1713, doi:10.1126/science.1081002.

Williams, K. D., and Coauthors, 2017: The Met Office Global Coupled Model 3.0 and 3.1 (GC3.0 and GC3.1) configurations. *Journal of Advances in Modeling Earth Systems*, **10 (2)**, 357–380, doi:10.1002/2017MS001115.

Williams, S. D., P. Moore, M. A. King, and P. L. Whitehouse, 2014: Revisiting GRACE Antarctic ice mass trends and accelerations considering autocorrelation. *Earth and Planetary Science Letters*, **385**, 12 – 21, doi:https://doi.org/10.1016/j.epsl.2013.10.016.

Yuan, N., M. Ding, J. Ludescher, and A. Bunde, 2017: Increase of the Antarctic sea ice extent is highly significant only in the Ross Sea. *Scientific Reports*, **7**, 41 096, article.

Zunz, V., and H. Goosse, 2015: Influence of freshwater input on the skill of decadal forecast of sea ice in the Southern Ocean. *The Cryosphere*, **9 (2)**, 541–556, doi:10.5194/tc-9-541-2015.

LIST OF TABLES

TABLE 1. Summary of experiment and control simulation settings. Note that these refer to Antarctic mass loss only, and the mass loss from Greenland remains as per the standard model configuration in all runs.

Simulation	Increasing Mass Loss	Icebergs	Ice Shelf Melt
PIControl	N	Y	Y
FW	Y	Y	Y
FWShelf	Y	N	Y
FWBerg	Y	Y	N

TABLE 2. Difference between the mean wind stress for each experiment and PIControl for the final 20 years of the simulations. The significance of any change is given by the p-value (following from calculation of the t-score for related samples). A p-value of less than 0.05 indicates a change significant at the 95% confidence level.

Experiment	Δ Latitude (°)	p-value	Δ Strength (Nm^{-2})	p-value
FW	-1.045	0.379	**0.019**	**0.011**
FWShelf	0.459	0.444	0.016	0.070
FWBerg	-0.208	0.929	0.004	0.943

LIST OF FIGURES

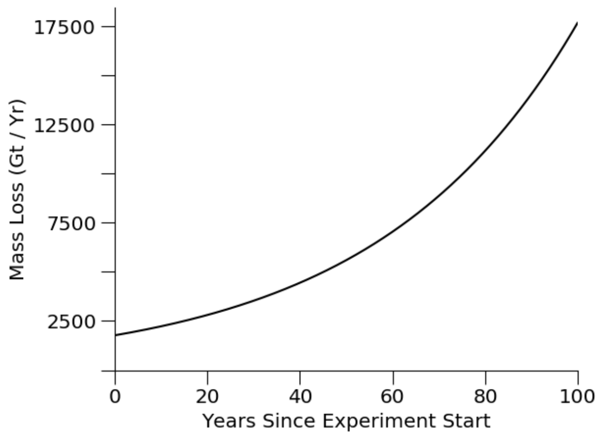

FIG. 1. The total rate of mass loss from the Antarctic continent in the experiments.